Marine Pollution Bulletin 80 (2014) 97–106

Contents lists available at ScienceDirect

Marine Pollution Bulletin

journal homepage: www.elsevier.com/locate/marpolbul

# Meteorologically-driven circulation and flushing times of the Bay of Algeciras, Strait of Gibraltar

José C. Sánchez-Garrido [a,*], Jesús García Lafuente [a], Simone Sammartino [a], Cristina Naranjo [a], Francisco J. de los Santos [b], Enrique Álvarez Fanjul [c]

[a] *Physical Oceanography Group, University of Málaga, Campus de Teatinos s/n, 29071 Málaga, Spain*
[b] *Autoridad Portuaria Bahía de Algeciras, Avda. de la Hispanidad 2, 11207 Algeciras, Cádiz, Spain*
[c] *Puertos del Estado, Avda. del Partenón 10, 28042 Madrid, Spain*

ARTICLE INFO

*Keywords:*
Bay of Algeciras
Wind-driven circulation
Tidal flushing
*e*-Flushing time
MITgcm

ABSTRACT

A primitive-equation model has been used to investigate the meteorologically-driven circulation of the Bay of Algeciras. It is shown that the mean circulation of Atlantic Water (AW) is characterized by an anticyclonic cell, while Mediterranean Water (MW) follows a preferred cyclonic pathway. Meteorological forcing distorts substantially the AW mean circulation pattern, and only modulates that of the MW. Winds drive a vertical circulation cell in the Atlantic layer consistent with Ekman dynamics, whereas the horizontal circulation pattern is markedly dependent on the swift Atlantic jet entering the Mediterranean and changes from clearly anticyclonic to cyclonic as the jet separates or approaches the strait's northern shoreline. This occurs through atmospheric pressure-driven acceleration/deceleration of the jet, in agreement with internal hydraulics theory predictions. It is also found that the renewal of AW is largely modulated by tides, with meteorological forcing playing a secondary role. The opposite applies to the renewal of MW.



## 1. Introduction

The Bay of Algeciras is located at the north-eastern end of the Strait of Gibraltar (Fig. 1). Covering an area of about $9 \times 11$ km, and with maximum depth of nearly 400 m, features by far the mildest surface currents of the strait. This circumstance has made this spot the preferred location in the zone for the settlement of harbors from early civilizations (Bernal Casasola et al., 2003). Today, the bay holds two important ports in both Algeciras and Gibraltar, and also numerous industrial plants distributed all along its shoreline. Marine pollution is therefore a realistic risk and a major problem in the area. A potential accident such as a significant oil spill will damage not only the remarkable ecology of the area, but also its economy and that of its surrounding regions, mainly depending on tourism.

Because of these factors the understanding of the bay's circulatory system is of particular concern, which has recently motivated a number of investigations. For instance, Álvarez et al. (2011) report on the existence of high-frequency motions related to the intrusion of an internal tidal bore coming from the main sill of the strait. Periñaez (2012) studied the dispersal of different types of pollutants, while recently Sammartino et al. (2014) described in detail both the barotropic and baroclinic tidal circulation of the bay in a combined numerical and experimental study.

Even if the major source of variability in the region are tides (García Lafuente et al., 2000), subinertial motions acting at typical time scales of 2–4 days can be also significant (see for instance Candela et al., 1989; García Lafuente et al., 2002). Broadly speaking, they are driven by local wind forcing, and more important, by fluctuations of atmospheric pressure in the far field (particularly over the western Mediterranean). Winds primarily affect the first tens of meters of the water column, while changes in atmospheric pressure lead to surface pressure gradients that drive barotropic flows through the Strait of Gibraltar. The associated volume transport can reach 1 Sv or more, and modulate substantially the exchange flow. An important effect of meteorologically forced flows is then expected on the bay circulation.

The aim of this paper is twofold. Firstly, to investigate the subinertial variability of the Algeciras Bay circulatory system; and second, to asses its flushing time under different meteorological and tidal scenarios. Regarding to this point, it should be noted that we use a more realistic approach than Periñaez (2012), who also aimed at providing typical flushing times of the bay on the basis of a barotropic tidal model. Note, however, that this is only a rough approximation as the actual (tidal and non-tidal) dynamics of the strait is markedly baroclinic (see, e.g., Sánchez-Garrido et al., 2011). Actually, Sammartino et al. (2014) show that Mediterranean

* Corresponding author. Tel.: +34 952132849.
*E-mail address:* jcsanchez@ctima.uma.es (J.C. Sánchez-Garrido).

0025-326X/$ - see front matter © 2014 Elsevier Ltd. All rights reserved.
http://dx.doi.org/10.1016/j.marpolbul.2014.01.036

and Atlantic Waters (MW and AW, respectively) in the bay, separated by a relatively pronounced pycnocline at around 90 m depth, present nearly counter-phase tidal motion.

This paper is organized as follows. Section 2 briefly describes the numerical model used in this work and its validation. Section 3 presents the model results, whereas Section 4 includes a short summary and some concluding remarks.

## 2. Numerical model

### 2.1. Model description

The Massachusetts Institute of Technology general circulation model (MITgcm; Marshall et al., 1997; Marshall et al., 1997) has been used in this work. We make use of the model simulation described in Sánchez-Garrido et al. (2013) and Sammartino et al. (2014), who developed a regional circulation model of the Strait of Gibraltar and adjacent sub-basins on the basis of the MITgcm source code. The model is a component of an operational oceanography system, and its detailed description can be found in the above referred papers; here we only give a brief outline of the model features and set up.

The model domain covers the Gulf of Cádiz and the Alboran Sea (from 9°W to 1°E), and has been discretized with an orthogonal curvilinear grid of variable horizontal resolution. It is maximum within the Strait of Gibraltar where $\Delta x$, $\Delta y \sim 300$–$500$ m. With this configuration the Bay of Algeciras contains $28 \times 25$ grid points. Towards the model open boundaries the resolution gradually decreases to 8–10 km. In the vertical, the model has 46 unevenly distributed *z*-levels. The resolution is maximum at the surface, $\Delta z = 5$ m, and exponentially decays towards the sea floor. The bottom topography is represented as partial vertical cells.

The model is laterally forced by daily-mean temperature, salinity and velocity fields extracted from a larger-scale circulation model of the Mediterranean (Oddo et al., 2009). Together with this slowly-varying forcing, tidal and meteorically-driven barotropic velocities are prescribed across the open boundaries. Tidal velocities are extracted from the results of the model described in Carrere and Lyard (2003), while the later velocity field, capturing the remote effect of atmospheric forcing in the model (essentially the inclusion of a barotropic flow through the strait varying at subinertial time scales), is obtained from the outputs of a storm surge operational system (Álvarez Fanjul et al., 2001). At the free surface the model is driven by high-resolution (1/20° in space, and 3 h in time) atmospheric forcing fields provided by the Spanish Meteorological Agency. Winds stress, shortwave, and longwave radiative forcing are applied to the ocean surface. Latent and sensible heat fluxes are interactively calculated by the model using standard bulk formulas.

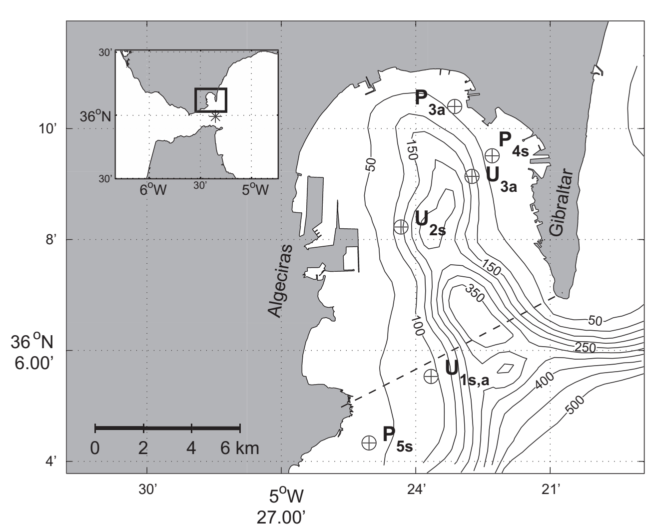


**Fig. 1.** Bathymetric chart of the Bay of Algeciras. The locations of the mooring lines deployed during the experiment are indicated and their respective names labelled. Subscripts indicate the season of the year when they were deployed: Spring(s) and Autumn (a). The asterisk mark in the inset indicates the location of the wind velocity time series referred in the text. Dashed line: bay mouth cross-section.

### 2.2. Model validation

The ability of the model to simulate a realistic variability of the exchange flow through the Strait of Gibraltar and the circulation of the Alboran Sea has been proven in Sánchez-Garrido et al. (2013). Regarding the Bay of Algeciras, Sammartino et al. (2014) found a very satisfactory agreement between model and field measurements at tidal scale, thus here we only focus on the subinertial time scale.

A set of moorings lines were deployed in the bay during Spring and Autumn 2011 (Fig. 1; see Sammartino et al., 2014 for detailed description of the experiments). In total 6 mooring lines were deployed, three of them at shallow depths (P3, P4, and P5; $\sim$25 m), and the rest (U1, U2, and U3) at around 100 m depth (subscripts "*s*" and "*a*" refer to Spring and Autumn respectively; same notation as in Sammartino et al., 2014). The low-frequency[1] temperature and salinity time series recoded near the sea floor are depicted in Fig. 2, together with the modelled time series. Overall, there is a very satisfactory agreement between model and observations. There are some discrepancies in the mean value of the time series, especially in salinity recorded at U1 (Fig. 2b), where the mean observed salinity exceeds in 0.33 units the modelled mean value. The difference is partially attributable to fine features of the bottom topography not represented by the model as the deepest model grid point at this location is some meters shallower than the depth of the CT probe. However, the model captures very well the amplitude and periodicity of the fluctuations of all the observed signals. The cross-correlation coefficient between observed and modelled variables ranges between $r = 0.78$ for salinity at U3, and $r = 0.95$ for temperature at T5, which are quite high values. It is also interesting to note the ability of the model for capturing the important fluctuations of temperature at shallow depths (Fig. 2a), driven by episodes of intense air-sea heat fluxes (not shown).

Fig. 3 shows the velocity over the two deepest stations of Spring (U1 and U2). Over U1 the zonal component (Fig. 3a) is predominantly negative over the whole water column and reaches peak values of around $-20$ cm s$^{-1}$ near the surface, where the signal appears substantially modulated and some sporadic events of velocity inversion occur. The meridional component (Fig. 3c) is of the same order but exhibits a noisier pattern. Its sign is mainly positive, which implies a quasi-permanent net flow towards the bay. Velocities over U2 are smaller, of the order of 5 cm s$^{-1}$ (Fig. 3e and g), and have a strongest dependence with depth, especially the zonal component that inverts sign at around 40 m and 80 m depth. It is positive near the surface and the bottom, and negative at mid-depths. It is interesting to note the prevalence of opposite sign of the near-surface velocities at U1 and U2, westwards and eastwards respectively, which suggests a dominant cyclonic circulation within the bay. As in U1, the meridional component has a more irregular pattern than the zonal velocity. The profiles are usually fairly homogeneous throughout the whole water column, alternating periods of northwards and southwards flow. The whole

[1] Low frequencies are meant here and throughout the rest of the paper as subinertial frequencies. The low-frequency signals are obtained by applying a low-pass Gaussian filter with cut off frequency of 0.5 days$^{-1}$ to the original time series.

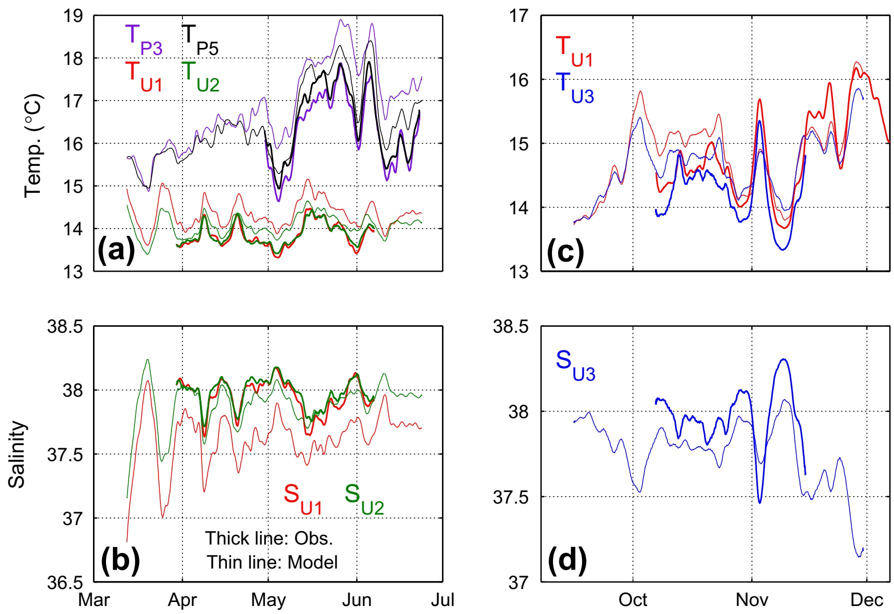


**Fig. 2.** Observed (thick line) and modelled (thin line) low-frequency temperature and salinity time series. A low-pass Gaussian filter with cut off frequency of 1/2 days$^{-1}$ has been applied to the original time series. Temperature at P4 is not shown because of failure of the ADCP Temperature Sensor (the time series follow a similar variability as the rest of shallow stations, but recording unrealistic colder temperatures). Salinity at U1 is not shown in panel d) (Autumn) because of complete failure of the CT probe.

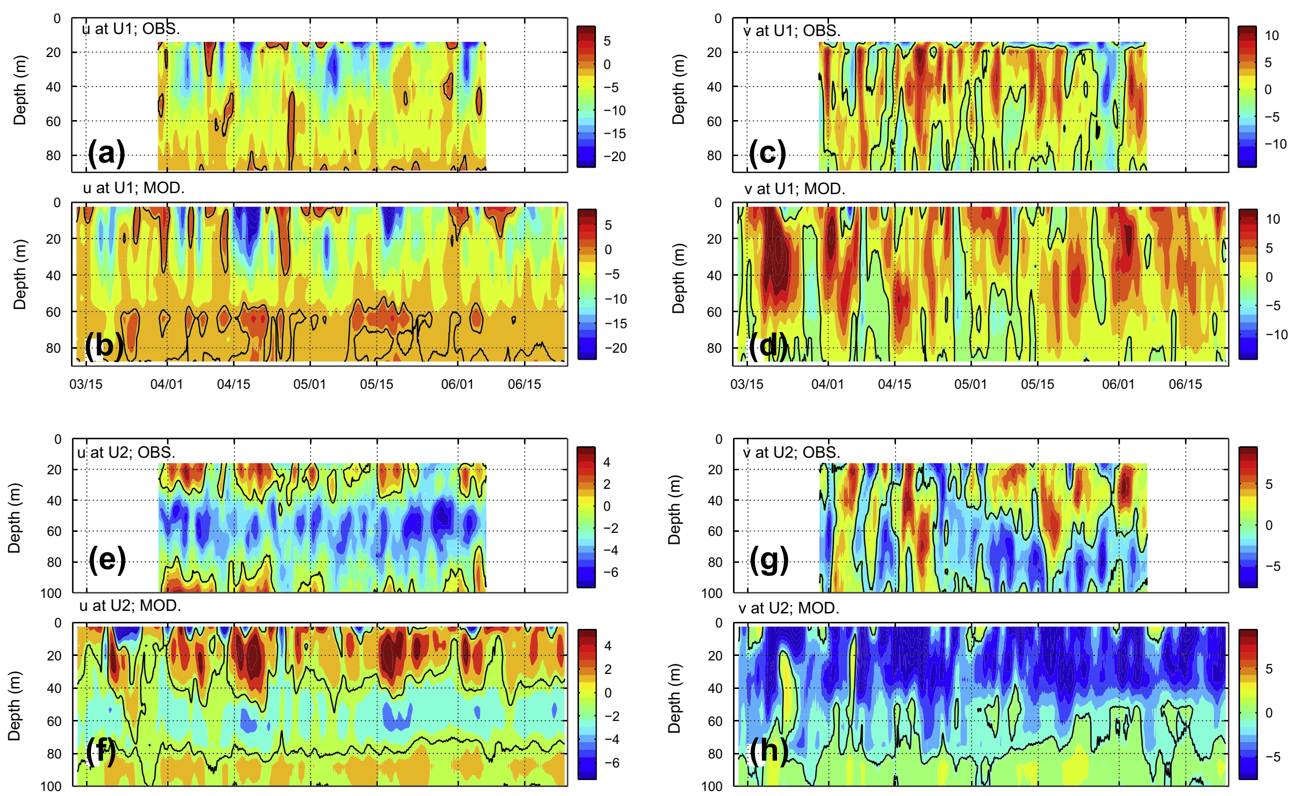


**Fig. 3.** (a and b) Observed and modelled low-frequency current velocity ($u$-component) over U1. The time series corresponds to Spring 2011. Units are in cm s$^{-1}$. The solid line is the zero-velocity contour. (c and d) Same as (a and b) for the $v$-component. (e and f) Same as (a and b) for U2. (g and h) Same as (e and f) for the $v$-component.

picture is successfully captured by the model (Fig. 3b, d, f, h); not only the magnitude but also the structure of vertical velocity profiles and the timing of the main flow intensification events. The exception of this agreement is the $v$ component at U2, where the model fails to capture episodes in which the flow turns to the north. At the shallow stations the agreement is also satisfactory (not shown), although not as much as in the deepest stations. This fact is probably the result of the poor representation of bottom and lateral friction with solid boundaries, which surely are dominant effects in these very shallow zones.

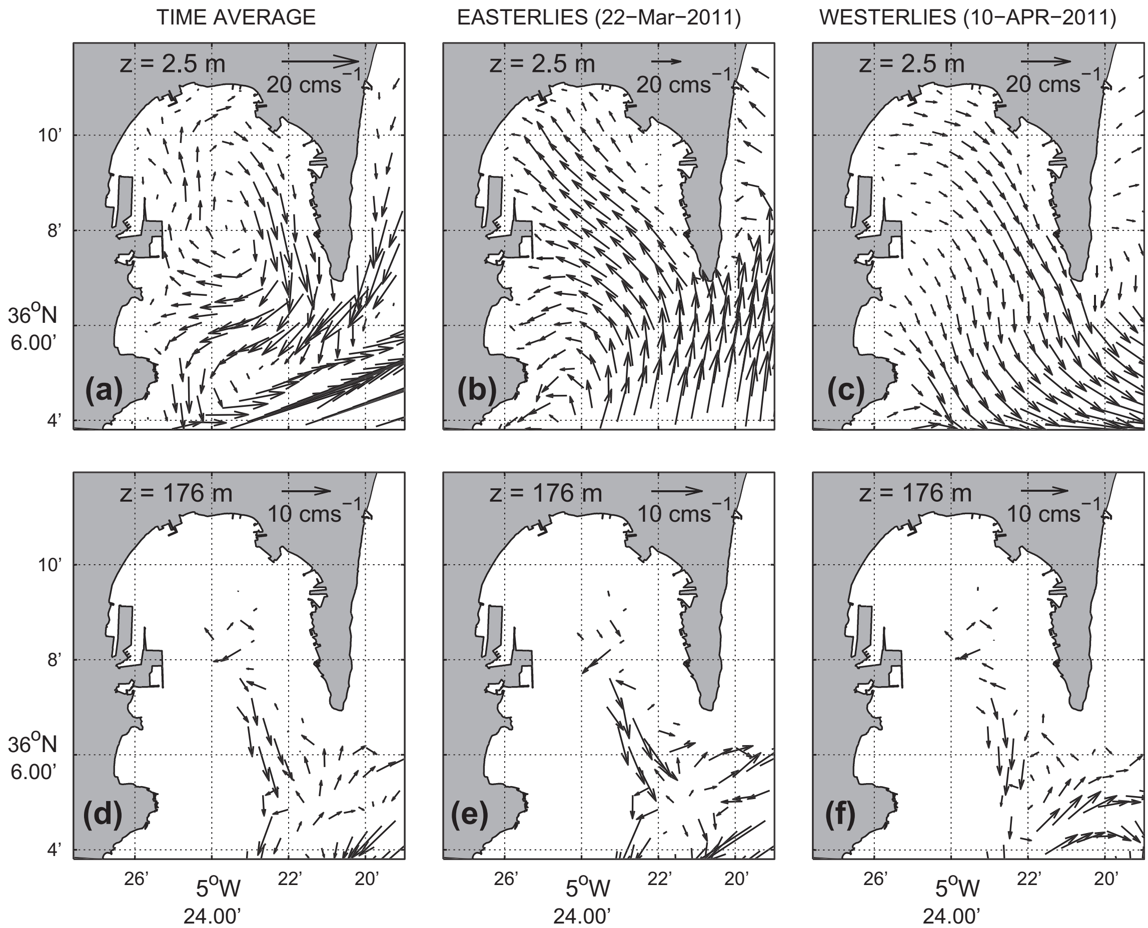


**Fig. 4.** (a) Time-average surface ($z = 2.5$ m) velocity field in the Bay of Algeciras (only 25% of the actual model velocity vectors are shown). (b) Surface velocity field during a particular event of easterly winds (March 22). A daily mean field is shown. (c) Same as (b) for westerly winds (April 10). (d–f) Same as (a–c) at $z = 176$ m.

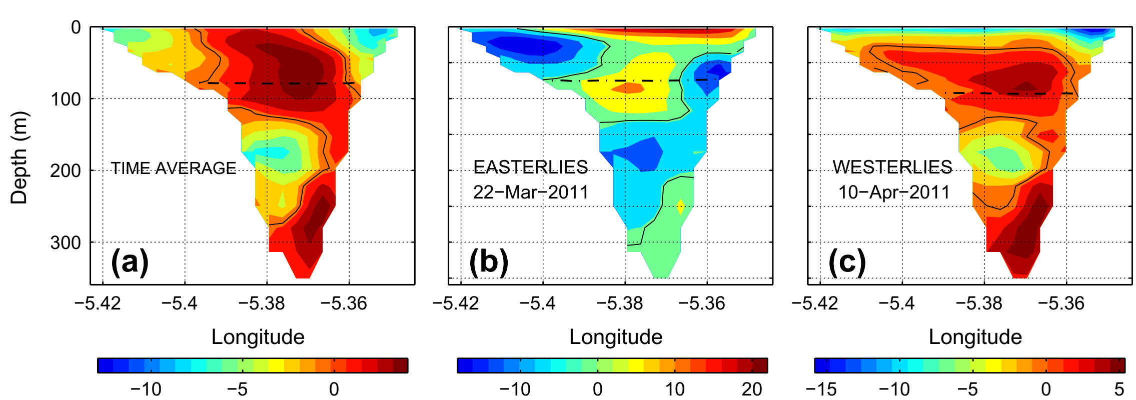


**Fig. 5.** (a) Time-average velocity across the mouth of the bay (units in cm s$^{-1}$, see exact cross-section in Fig. 1). Positive (negative) values indicate velocities inward (outward) the bay. The solid line is the zero-velocity contour. The dashed line is the isopycnal surface $S = 37.5$ (nearly coincident with the pycnocline). (b) Same as (a) during a particular event of easterly winds (March 22). A daily-mean field is shown. (c) Same as (b) for westerly winds (April 10).

Velocities recorded in Autumn are modelled with similar level of accuracy. Velocity profiles at U1 (not shown) are similar to those of April, thus suggesting a weak seasonal variability of the circulation. Model results also indicate so. In the following we will focus on the analysis of a hindcast simulation for Spring, bearing in mind that the results are essentially applicable to any other period of the year.

## 3. Results

### 3.1. Mean circulation and variability

This Section is intended to describe the mean circulation of the bay and its variability under dominant wind conditions. The time average surface velocity field is characterized by an anticyclonic

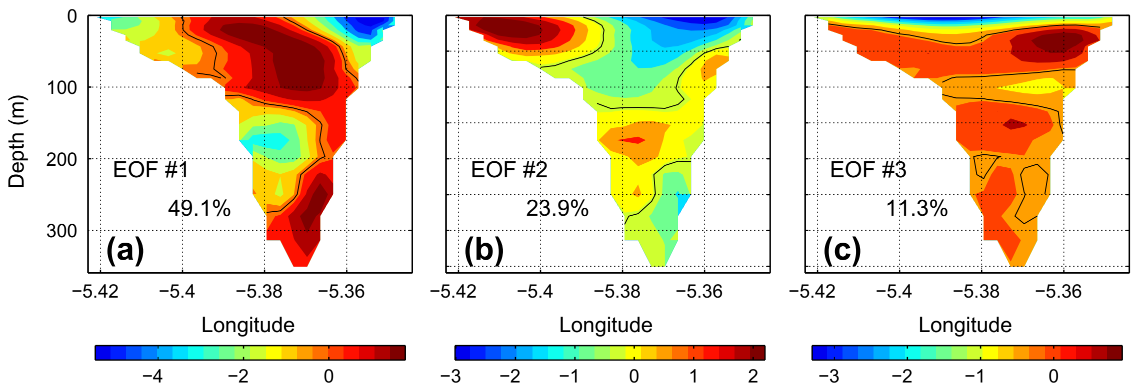


**Fig. 6.** First three EOFs of the low-frequency velocity time series across the mouth of the bay. Solid line is the zero-velocity contour. The percentage of the corresponding explained variance is labelled.

cell (Fig. 4a) that encompasses the whole bay. It is isolated from the Atlantic Jet (AJ; swift current at the bottom right corner of the figure) by a coastal counter-current that runs along the eastern side of the rock of Gibraltar. Within the Mediterranean layer, at $z = 176$ m, MW leaves the bay through the western side of the canyon, whereas a weaker current enters through its eastern side. Fig. 5a shows the velocity field across the mouth of the bay (see Fig. 1), and provides a new insight of the circulation. The dashed contour is the isohaline $S = 37.5$, which as noted by Sammartino et al. (2014) nearly coincides with the pycnocline in this part of the strait, and is therefore taken as the interface between AW and MW. AW enters the bay through the center of the mouth, and leaves through its lateral boundaries. Observing the surface circulation pattern, it becomes apparent that only water particles exiting trough the west of the bay mouth are incorporated into the AJ to definitely leave the bay; those exiting from the east will apparently recirculate and eventually enters the bay through the its central part. At depth, MW exits the bay through a core located over the western slope and centred at 190 m depth.

The actual circulation is unsteady though, and the described pattern is only representative of a hypothetical mean state. Let us, for instance, explore how it is modified during two particular events of strong easterly (March 22; Fig. 1), and westerly winds (April 10; Fig. 4c). With the easterlies the anticyclonic cell that characterized the mean surface circulation has been replaced by a quite unidirectional current towards the head of the bay, and the opposite occurs under westerlies, surface water is drained from the bay. This is the expected result of the Ekman drift effect.

The resulting horizontally divergent surface flow is, at least partially, compensated for an undercurrent (Fig. 5b and c) of AW, which under westerlies looks more homogeneously distributed across the bay mouth. Regarding the Mediterranean layer, easterlies force MW to leave the bay, especially through the above mentioned core, which now is larger than in the mean field (Figs. 4e and 5b). The opposite occurs during westerlies (Figs. 4f and 5c). Therefore, winds seem to regulate the amount of AW and MW present in the bay; easterlies (westerlies) tend to fill the bay with AW (MW), and drain MW (AW). We shall see later in more detail that this is the case.

### 3.2. Renewal patterns

The former examples reveal a substantial variability of the bay circulation induced by winds. In particular, it is interesting to note that the structure of the velocity field in the Atlantic layer is qualitatively different from easterlies to westerlies across the bay mouth. AW is essentially renewed in the vertical during the westerly event, resembling an estuarine exchange. In the case of the easterly wind, the flow exhibits an important horizontal structure overimposed to the vertical pattern, with water entering through the east of the mouth, and leaving through its western flank. Motivated to understanding what drives these patterns, an Empirical Orthogonal Function (EOF) analysis has been applied to the velocity time series across the mouth of the bay. The most significant spatial modes or EOFs (explaining a combined 85% of the variance) are displayed in Fig. 6, and their temporal coefficients or Principal Components (PCs) in Fig. 7.

Let us focus first on EOF #3. It is characterized by a very active surface layer of 10–15 m thick, and the associated PC is highly correlated with the low-frequency zonal component of the wind stress, $\tau_x$ ($r = 0.78$; Fig. 7c), from which we can conclude that this EOF is mainly capturing the spatial pattern produced by wind

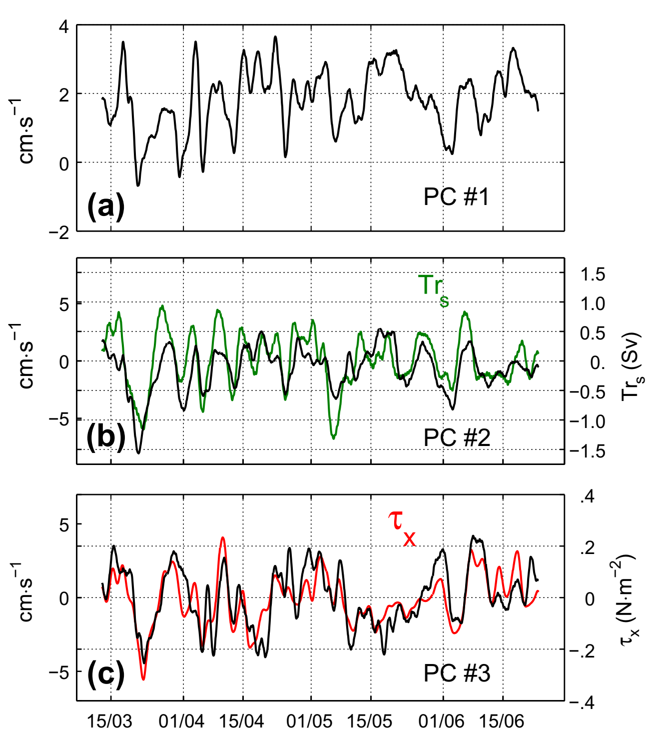


**Fig. 7.** First (a), second (b) and third (c) PCs of the low-frequency velocity time series across the mouth of the bay (units in cm s$^{-1}$). The green and red line in panels (b and c) are $Tr_s$ and $\tau_x$, respectively (units on the right of the axes). (For interpretation of the references to color in this figure legend, the reader is referred to the web version of this article.)

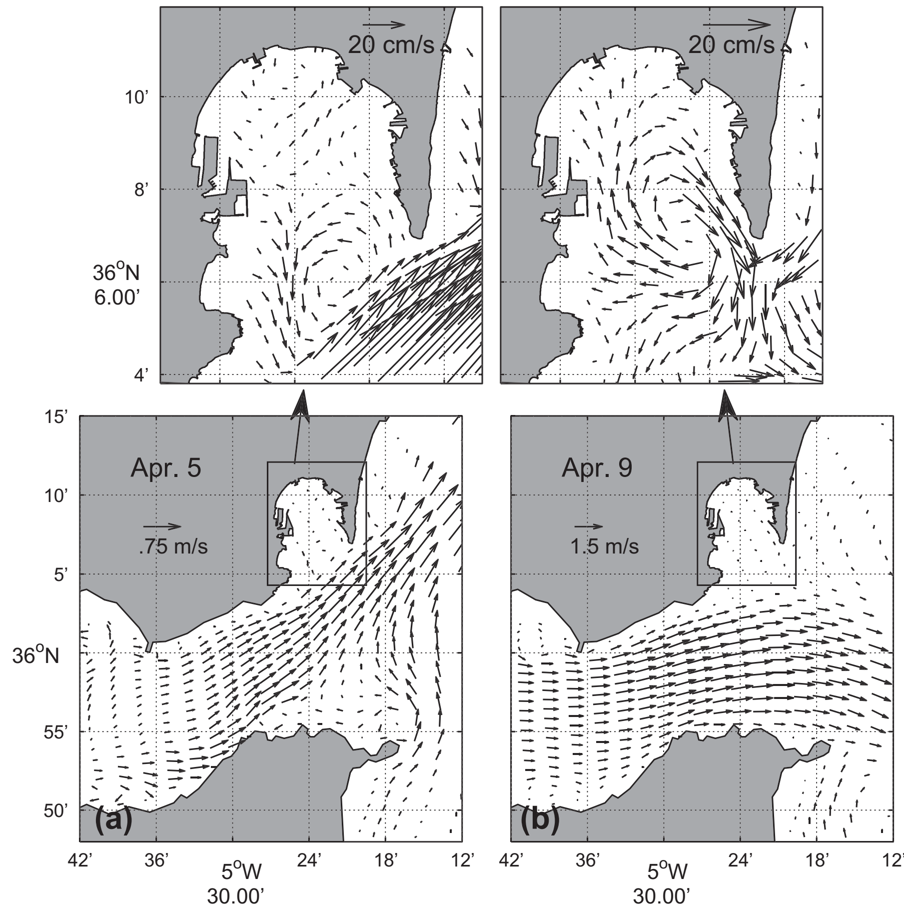


**Fig. 8.** (a) Daily mean velocity field at $z$ = 27.5 m depth on April 5. The low-frequency net transport at that time was $Tr_s = -0.78$ Sv (see Fig. 7b). The panel on top shows a close-up of the bay area. (b) Same as (a) for April 9. $Tr_s = 0.82$ Sv.

stress forcing. Note that velocities across the section have different sign to those in the very surface layer except for a thin strip centred at the interface (around 100 m depth). This fact has two important implications. First, winds activate a vertical circulation cell within the Atlantic layer, and second, winds modulate the volume of Atlantic and Mediterranean water in the bay. Looking at the structure of EOF #3 it can be noted that easterly winds cause a negative (oceanwards of the bay) net MW volume transport. The reason is that the exchange of AW in the upper layer is not completely in balance; there is a net transport that during easterly winds fills up the bay with AW and forces MW to flow out. The opposite occurs during westerlies. More details and evidence of this process are given in the next section.

The second EOF captures a marked horizontal renewal pattern of AW, and also regulates the renewal of MW through the modulation of the MW core size. The corresponding PC is typically negative (positive) during easterlies (westerlies), which implies a cyclonic (anticyclonic) circulation anomaly within the Atlantic layer (Fig. 7b). Although some correlation between this PC and $\tau_x$ is certainly apparent, the correlation coefficient is not as high as in the case of PC #3 ($r = 0.34$ against $r = 0.78$), which suggests that winds do not control, at least completely, this circulation pattern. This fact is also suggested by the own characteristics of EOF #2. It captures fairly strong currents within the first 50 m, while typically winds only affect substantially the circulation of the surface 10–20 m layer (much like in EOF #3), a typical thickness of the Ekman layer.

We anticipate that subinertial fluctuations of the net flow through the Strait of Gibraltar controls the variability of EOF #2. Its volume transport, $Tr_s$, is shown in Fig. 7b and is highly correlated with PC #2 ($r = 0.69$). The explanation can be found in Fig. 8 that depicts the velocity field at 27 m depth, below the thin surface layer in which the effect of wind forcing is dominant. Inspection of the model outputs reveals that when $Tr_s < 0$ (flow towards the west) as in Fig. 8a (April 5, $-0.78$ Sv), the AJ is slowed down, and more important, it approaches the mouth of the bay. The result is that the coastal current that in a typical situation runs westwards along the eastern side of Gibraltar (Fig. 4a), is blocked by the AJ. Actually, the AJ can flow so close to the coast that might partially impinge against the southern tip of Gibraltar, to later intrude into the bay through its eastern side as a result of the flow-topography interaction. This situation leads to a cyclonic circulation of AW in the bay (see inset map on top of Fig. 8a). On the other hand, when $Tr_s > 0$ (net flow towards the east, as in April 9, 0.82 Sv; see Fig. 8b), the AJ accelerates and separates from the bay, thereby facilitating the intrusion of the coastal counter-current that enhances the mean anticyclonic circulation.

The separation of the AJ from the northern coast of the strait has been addressed in a number of papers dealing with the hydraulics of the exchange flow (see Timmermans and Pratt, 2005 and the references therein), all of them linking the flow separation event with the presence of a supercritical AJ. This is exactly what the model results suggest as the separation takes place when the jet accelerates. The issue is interesting by itself and deserves an in-depth analysis that is beyond the scope of this paper. Here we only remark that our model results support this theoretical result, and certainly has important consequences for the bay circulation.

Lastly, note that EOF #1 has the same structure as the mean velocity field (the time average was not removed from the original series). Generally, it is the dominant pattern, but there are a number of episodes when it vanishes (PC #1 becomes null). This occurs when $Tr_s$ is significantly negative (compare Figs. 7a and b). In these situations it is EOF #2 that dominates the general spatial pattern.

### 3.3. Flows and water budget

We now explore the low-frequency variability of the flow through the bay and its water masses budget. The AW and MW volume transport across the mouth is depicted in Fig. 9. We show separately inward (positive), outward (negative), and net (positive plus negative) flows. The mean value of the AW exchange transport is $3.23 \cdot 10^{-2} \pm 6.61 \cdot 10^{-3}$ Sv, and slightly less in the case of MW, $3.08 \cdot 10^{-2} \pm 5.23 \cdot 10^{-3}$ Sv. In both layers, inward and outward flows are in balance in the long term, but at a given time they do not compensate each other. Typically there exists a net flow of the order of $\sim 1 \cdot 10^{-3}$ Sv, one order of magnitude smaller than the flow that is exchanged. The divergence causes the drainage or replenishment of the bay with the corresponding water. Obviously, as volume is preserved in the bay except for small divergences that cause free surface elevation anomalies of few centimeters (storm surge), the net flow through the two layers are in counter-phase, and also their corresponding volumes (Fig. 9b). Fluctuations in MW and AW budgets, in turn, cause vertical displacements of the isopycnals, which are responsible for the oscillations of temperature and salinity signals observed at locations U1 and U2 (Fig. 2). For instance, the high correlation between salinity at U1 and the net flow through the Atlantic layer, $r = -0.94$, makes it clear.

Winds regulate the water masses budget. Easterlies accumulate surface water in the bay that fills the Atlantic layer and forces the drainage of MW. Westerlies produce the opposite. This mechanism is supported by the significant correlation between $\tau_x$ and the net flow of AW, $r = -0.48$, which increases further to $r = -0.70$ between $\tau_x$ and the Atlantic layer volume when a time shift of 74 h is applied to the later.

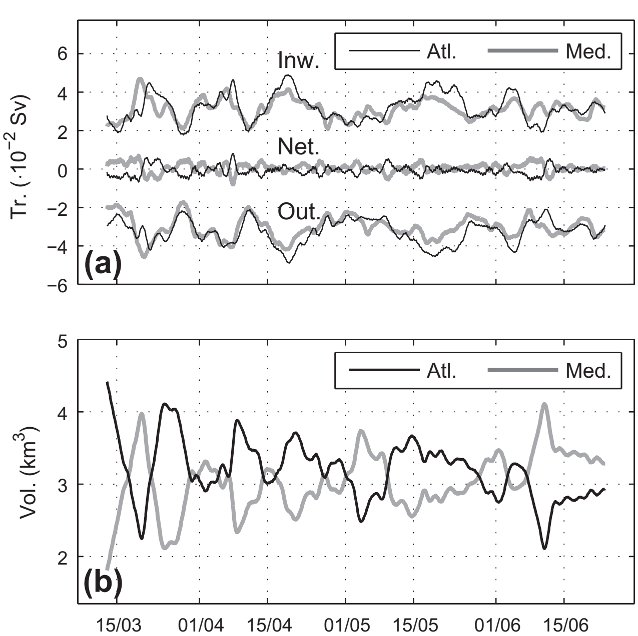


**Fig. 9.** (a) Volume transport of AW (black line) and MW (gray line) across the mouth of the bay. Inward, outward and net (inward plus outward) transports are shown. (b) Temporal evolution of Atlantic (black line) and Mediterranean (gray line) water volume in the bay.

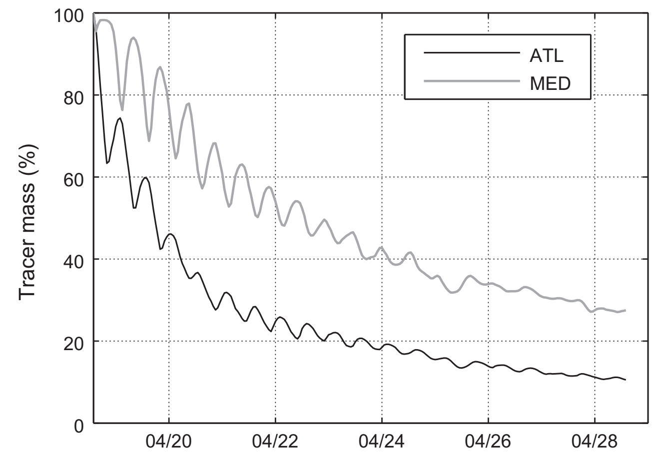


**Fig. 10.** Temporal evolution of passive tracers content in the bay (in % of their initial amount). Black (gray) line corresponds to a tracer initially released within the Atlantic (Mediterranean) layer. Tracers were released on April 18, 14:00 h.

One also might think about the role of the flow variability through the Strait of Gibraltar in regulating the water budget of the bay, as it substantially affects its circulation. There are two arguments that indicate that it is small. First, the circulation pattern induced by changes of $Tr_s$ in the bay is mainly horizontal in the Atlantic layer, which means that it can be horizontally non-divergent and therefore it does not involve vertical motions. Note that this is not the case of the wind-driven circulation, which is horizontally divergent in the surface layer and thereby induces a downward vertical motion necessary to drain MW. Second, the correlation between $Tr_s$ and the net flow of AW is smaller, $r = -0.31$, being probably still moderate due to the own correlation between $Tr_s$ and $\tau_x$. [2]

### 3.4. Residence time

On the basis of the low-frequency flows, the residence time of a fluid particle in a specific layer can be estimated by $t_{res} = V/Tr$, where $V$ is its volume and $Tr$ the volume transport. We are assuming here that the Atlantic and Mediterranean layers are immiscible within the bay, so that particles initially within one layer cannot eventually become part of the other. Even in coastal regions, typical mixing processes do not modify substantially water properties during periods of time shorter than some days, so we can consider that AW and MW are immiscible in the bay as long as the estimated residence time is of this order. Indeed, the layer volumes are $V \sim 2–4 \cdot 10^9$ m$^3$, and $Tr \sim 2–5 \cdot 10^4$ m$^3$ s$^{-1}$, which gives a $t_{res}$ fluctuating between 0.5 and 2.3 days depending on meteorological forcing.

These values come with very important caveats though. First, it should be noted that the estimate is formally applicable to steady or quasi-steady flows, in which the flow and the water body volume in question change at much smaller time scales than $t_{res}$. This condition is not fulfilled here, as the variation time scale of $Tr$ is 2–3 days, approximately the value of $t_{res}$. Second, it is also assumed that fluid particles that leave the bay do not eventually return. The flow across the mouth of the bay, especially within the Atlantic layer, is often part of the branch of a cyclonic or anticyclonic cell, thus recirculation is indeed expected. In addition, and more

[2] In the Strait of Gibraltar both winds and the subinertial net flow usually point at the same direction. A high-pressure (low-pressure) system over the western Mediterranean is usually accompanied by the onset of easterly (westerly) winds in the strait, and also by a positive (negative) pressure anomaly over the ocean free surface that causes a westward (eastward) flow.

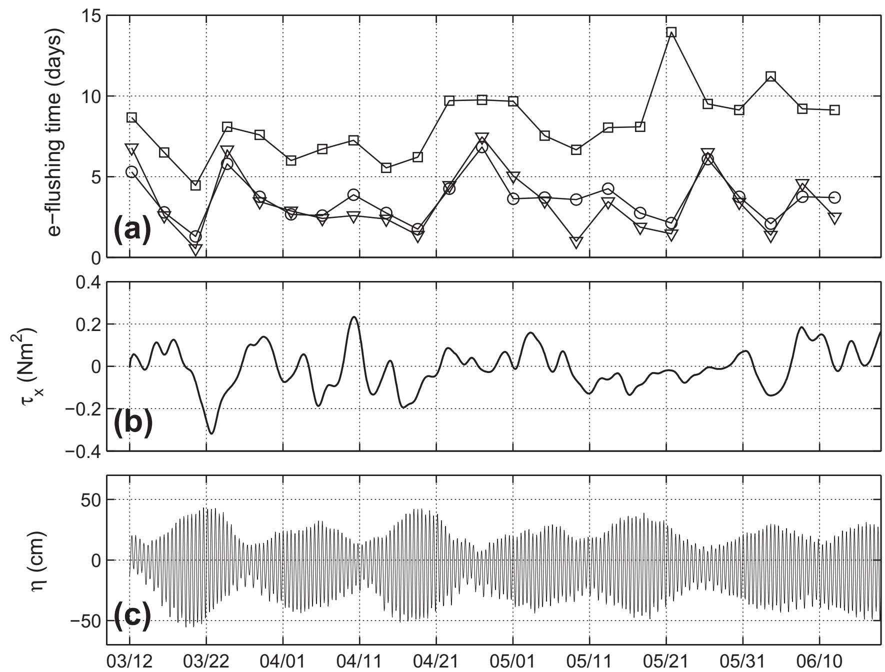


**Fig. 11.** (a) Temporal dependence of the Atlantic (circles), Mediterranean (squares), and surface ($-5 < z < 0$ m; triangles) layer *e*-flushing times. The marks are located at the time of the passive tracers release. *e*-flushing times greater than 10 days were calculated by exponential extrapolation. (b) Low-pass filter $\tau_x$ time series. (c) Sea surface height at U1.

importantly, we are neglecting here the pulsating effect of tides. Recall that tides are the main source of variability thus they are expected to play a relevant role in the bay renewal process (Sammartino et al., 2014).

A more suitable approach to assess how efficiently the bay is renewed and the dominant mechanisms involved consists in sequentially launching Lagrangian drifters, and make some statistics of their particular residence time. A second possibility is the consideration of passive tracers, governed by the advection–diffusion equation. This approach is followed next, and a measure of the ventilation will be given in terms of the *e*-flushing time, that is, the time required for the initial tracer concentration to be reduced by a factor of *e*.

### 3.5. e-Flushing times

A number of experiments using passive tracers were carried out in order to asses the *e*-flushing time of the bay under different flow conditions. In total, 44 independent tracers were released throughout the simulation, two every four days or so. In every experiment we considered an Atlantic and a Mediterranean tracer. In the first, we prescribed a tracer concentration equal to unity within the Atlantic layer, and zero in the rest of the domain. In the Mediterranean tracer the set up was similar but with tracer concentration equal to one in the Mediterranean layer. All tracers were released at the same stage of the tidal cycle, at high tide in particular, in order to make all the experiments strictly comparable. After their release, the evolution of every individual tracer was tracked during the subsequent 10 days.

Fig. 10 shows the mass[3] of two particular tracers contained in the bay with respect to their initial value. Black and gray lines correspond to an Atlantic and Mediterranean tracer, respectively, launched at the same time. Both curves decay following an exponential-like law, with riding oscillations of semidiurnal periodicity caused by tidal motions. These oscillations are in counter-phase along the two curves, a fact that makes clear the baroclinic character of the tides.

Generally the Atlantic curve decays more rapidly than the Mediterranean, thus it can be stated that the Atlantic layer is renewed more efficiently (*e*-flushing time of ∼2 against ∼6 days). Note, however, that the final difference of tracer mass content is mainly achieved during the first 3–4 days of evolution, when the decay rate of the Atlantic curve is particularly pronounced. Later during the second part of the experiment the two curves decay nearly at the same rate. The transition from these two differentiable periods is characterized by changing tides from spring to neap (see Fig. 11c).

The different behavior of the two tracers with tides becomes apparent by a close inspection of the oscillations along the mass curves. For the Mediterranean tracer the fluctuations look quite harmonic, so that at tidal scale nearly every fluid particle that comes out returns to the bay when the tidal flow reverses. In the Atlantic layer, however, much smaller fraction of the tracer mass that leave the bay with the tidal flow is recovered with its reversal. This is explained by the swift Atlantic currents present in this part of the strait. When a water parcel leaves the bay encounters strong currents, so the probability to be advected far enough to do not return when the tidal flow inverts is high. On the other hand, Mediterranean currents in this region of the strait are much weaker, and this makes the probability of the particles return higher. This behavior can be clearly observed in the digital auxiliary material.

In all the experiments the Atlantic layer is renewed more efficiently than the Mediterranean. The *e*-flushing times of the two layers is $3.61 \pm 1.39$ and $8.20 \pm 2.05$ days, respectively (circle and square marks in Fig. 11). The difference is, as noted before, due to tides. If we look at a particular layer it can be noted that its *e*-flushing varies significantly in time. For example, the three minimum *e*-flushing times in the Atlantic are achieved on 03/21, 04/19, 06/04; and the maximum values on 03/25, 04/28, and 05/26.

[3] $\int_V C\,dV$, where $C$ is the tracer concentration, and $V$ the bay volume.

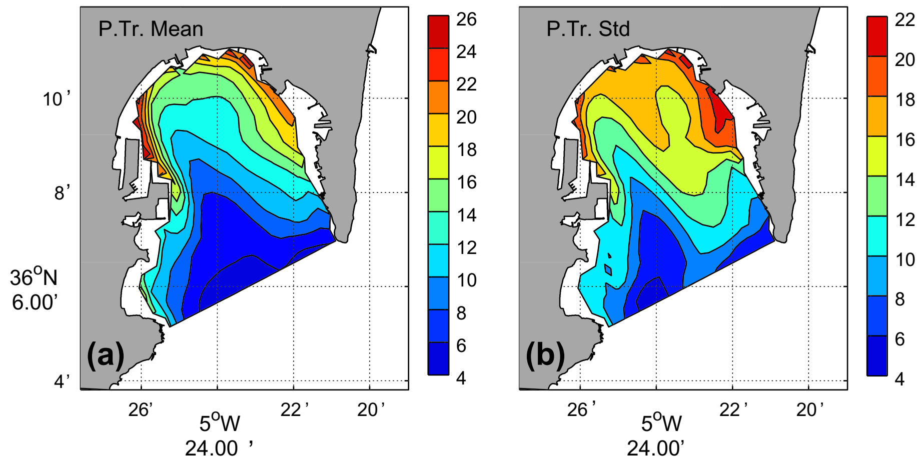


**Fig. 12.** Time average (a) and standard deviation (b) of tracer mass in the surface layer after 7 days of evolution (% with respect its initial value).

Maximum and minimum values, of approximately 1 and 7 days, coincide in time with spring and neap time periods, respectively, which indicates that tides strongly regulate the ventilation of this layer. Winds (Fig. 11b) also seem to introduce some modulation, but small in comparison to tides. To illustrate this, consider the tracers launched between 05/18 and 05/21, under calm wind conditions but also encountering intense tidal currents. The corresponding *e*-flushing time is hardly 1 day greater than the three minimum values, which were all coincident in time with the presence of strong easterly winds (Fig. 11b).

By contrast, the ventilation of the Mediterranean layer is not especially controlled by tides, but rather by meteorological forcing. To note this, consider now the period from 03/22 to 04/11. Within this period, which includes more than a fortnightly tidal cycle, the Mediterranean *e*-flushing times barely change. It does, however, increase noticeably from the first half of the simulation (until 04/21) to the second half. During the first period winds and in less degree, $Tr_s$, exhibit more variability, thus suggesting that it is indeed meteorological forcing that control the renewal of MW.

For practical applications, it is particularly interesting to look at the model surface layer. Its mean *e*-flushing time value is only slightly shorter than that of the Atlantic layer as a whole, $3.40 \pm 1.98$ days, and their temporal dependence very similar (triangles in Fig. 11a). Fig. 12a shows the mean spatial distribution of tracer mass after 7 days of evolution, and provides a map of stagnant and dynamical regions. As expected, the bay is ventilated less and less efficiently as one moves from the mouth to the head, with the most stagnant areas confined along the lateral boundaries (concentration of around 25%). In addition to this meridional gradient, the mass values also vary slightly from west to east, indicating that the western flank of the bay is better ventilated. Its northeastern quadrant is in average the most stagnant one, but also the one in which the tracer concentration varies the most during the simulation (Fig. 12b).

## 4. Summary and concluding remarks

In this study we described the meteorological forced subinertial circulation of the Bay of Algeciras. The analysis is based on the results of a numerical simulation of the bay circulation that satisfactorily compared quantitatively and qualitatively with observations.

The mean circulation of the bay is anticyclonic in the Atlantic layer, and cyclonic in the Mediterranean. These patterns are distorted by winds and meteorological-driven flows through the Strait of Gibraltar. Winds drive a vertical circulation that extends across the whole Atlantic layer in line with what is expected from Ekman dynamics, i.e., upwelling during westerlies, and downwelling with easterlies. Winds also regulate the amount of AW (and consequently also that of MW) present in the bay, draining it during westerlies and filling the bay with it during easterlies. Fluctuations of the barotropic flow through the Strait of Gibraltar, on the other hand, enhance or diminish (even revert) the prevalent anticyclonic trajectory of AW. This occurs through the approximation or separation of the AJ from the bay as it accelerates or slows down, in agreement with internal hydraulics predictions.

We also concluded that flushing times of the Atlantic layer are largely modulated by tidal currents, and that the effect of meteorological forcing is weak in comparison. Flushing times of the Mediterranean layer are less variable than the Atlantic, and do not show a substantial dependence on tides, whereas the surface layer is renewed in a similar fashion as the Atlantic layer as a whole. Overall, we obtain an average bay flushing time (Atlantic plus Mediterranean layers) of approximately 10 days, which is about half the value given by Periñaez (2012) for conservative pollutants. Our greater predicted flushing rate is attributable to the presence of the AJ in our model which, as it has been argued, enhances the bay ventilation process through the rapid scattering and eastward advection (to the Alboran Sea) of tracer particles as they exit the bay with tidal pulses. The AJ is a baroclinic feature and consequently was not present in the barotropic model of Periñaez (2012). This explains the apparent surprising result of this author, who pointed out that flushing of the bay is not as fast as it could be expected from the strong currents in the Strait of Gibraltar.

Lastly, it is convenient to stress that our flushing time estimates, particularly those of the very surface layer of the bay, have been made by means of passive tracers, that is, by means of particles of neutral buoyancy that do not receive direct momentum from winds. Some differences can then be expected when applying more sophisticated oil spill models.

## Acknowledgements

The model runs and the experimental data analyzed in this work have been provided within the frame of the SAMPA project, funded by the Spanish institutions of Autoridad Portuaria Bahía de Algeciras and Puertos del Estado. Partial financial support was provided by the Spanish funded INGRES project (CTM2010-21229-C02-01/MAR, Ministerio de Economía Competitividad). CN acknowledges the pre-doc fellowship BES-2011-043421. We are also grateful to Cádiz and Granada Universities and Instituto

Hidrográfico de la Marina for their support in the field experiments. Special thanks to the crew of Calima ship from the Port Authority of the Bay of Algeciras, on board of which the field experiments were carried out. Supercomputing facilities of the SCBI center, University of Malaga, are also acknowledge. This is the publication no. 49 from CEIMAR Publication Series.

## Appendix A. Supplementary data

Supplementary data associated with this article can be found, in the online version, at http://dx.doi.org/10.1016/j.marpolbul.2014.01.036.

## References

Álvarez, O., González, C.J., Mañanes, R., López, L., Bruno, M., Izquierdo, A., Gómez-Enri, J., Forero, M., 2011. Analysis of short-period internal waves using wave-induced surface displacement: a three-dimensional model approach in Algeciras Bay and the Strait of Gibraltar. J. Geophys. Res. 116.

Álvarez Fanjul, E., Pérez Gómez, B., Rodríguez Sánchez, A.I., 2001. Nivmar: a storm surge forecasting system for Spanish waters. Sci. Mar. 65 (S1), 145–154.

Bernal Casasola, D., Jiménez Camino, R., Lorenzo Martínez, L., Torremocha Silva, A., Expósito Álvarez, J.A., 2003. Las factorías de salazones de Iulia Traducta. Almoraima 29, 163–184.

Candela, J., Winant, C.D., Bryden, H.L., 1989. Meteorologically forced subinertial flows through the Strait of Gibraltar. J. Geophys. Res. 94 (C9), 12667–12679.

Carrere, L., Lyard, F., 2003. Modelling the barotropic response of the global ocean to atmospheric wind and pressure forcing – comparisons with observations. Geophys. Res. Lett. 30 (6), 1–8.

García Lafuente, J., Vargas, J.M., Plaza, F., Sarhan, T., Candela, J., Bascheck, B., 2000. Tide at the eastern section of the Strait of Gibraltar. J. Geophys. Res. 105 (C6), 14197–14213.

García Lafuente, J., Álvarez Fanjul, E., Vargas, J.M., Ratsimandresy, A.W., 2002. Subinertial variability in the flow through the Strait of Gibraltar. J. Geophys. Res. 107 (C10), 3168.

Marshall, J., Hill, C., Perelman, L., Adcroft, A., 1997. Hydrostatic, quasi-hydrostatic, and nonhydrostatic ocean modeling. J. Geophys. Res. 102 (C3), 5733–5752.

Marshall, J., Adcroft, A., Hill, C., Perelman, L., Heisey, C., 1997. A finite-volume, incompressible Navier Stokes model for studies of the ocean on parallel computers. J. Geophys. Res. 102 (C3), 5753–5766.

Oddo, P., Adani, M., Pinardi, N., Fratianni, C., Tonani, M., Pettenuzzo, D., 2009. A nested Atlantic–Mediterranean sea general circulation model for operational forecasting. Ocean Sci. 5, 461–473.

Periñaez, R., 2012. Modelling the environmental behaviour of pollutants in Algeciras Bay (South Spain). Mar. Pollut. Bull. 64, 221–232.

Sammartino, S., García-Lafuente, J., Sánchez-Garrido, J.C., de los Santos, F.J., Álvarez-Fanjul, E., Naranjo, C., Bruno, M., Calero, C., 2014. A numerical model analysis of the tidal flows in the Bay of Algeciras, Strait of Gibraltar. Cont. Shelf Res. 72, 34–46.

Sánchez-Garrido, J.C., Sannino, G., Liberti, L., García Lafuente, J., Pratt, L., 2011. Numerical modeling of three-dimensional stratified tidal flow over Camarinal Sill, Strait of Gibraltar. J. Geophys. Res. 116, C12026. http://dx.doi.org/10.1029/2011JC007093.

Sánchez-Garrido, J.C., García-Lafuente, J., Álvarez-Fanjul, E., García Sotillo, M., de los Santos, F., 2013. What does cause the collapse of the Western Alboran Gyre? results of an operational ocean circulation system. Prog. Oceanogr. 116, 142–153.

Timmermans, M-L.E., Pratt, L.J., 2005. Two-layer rotating exchange flow between two deep basins: theory and application to the Strait of Gibraltar. J. Phys. Oceanogr. 35, 1568–1592.